1-2013

Modeling of Chemical Nonequilibrium Effects in a Charring Ablator

Alexandre Martin
University of Kentucky, alexandre.martin@uky.edu

Digital Object Identifier (DOI)
http://dx.doi.org/10.2514/6.2013-301

51st AIAA Aerospace Sciences Meeting including the New Horizons Forum and Aerospace Exposition
07 - 10 January 2013, Grapevine (Dallas/Ft. Worth Region), Texas

AIAA 2013-0301

Modeling of chemical nonequilibrium effects in a charring ablator

Alexandre Martin*

Department of Mechanical Engineering, University of Kentucky, Lexington, KY

Charring ablators remain the premium choice for space exploration missions that involve atmospheric re-entry. These type of ablative material are composed of a carbon matrix, usually made of fibers, which is then impregnated with a resin. During re-entry, the high heat flux produced by convective heating causes the material to chemically react. First, the resin pyrolyzes, and is vaporized into a gas that travels through the material, and is eventually ejected at the surface. Since the composition of the gas at the surface greatly affects the heat flux, and therefore the surface temperature, it is thus important to be able to accurately predict its composition.

When the temperature becomes high enough, the surface of the ablator also vaporizes. That phenomenon is of much concern when sizing Thermal Protection Systems (TPS): for instance, if the recession is severe, the shape of the vehicle could be altered, as would be the aerodynamics properties.

The research presented here demonstrates two physical models that have been integrated into a material response code that aims at predicting surface recession more accurately. First, a non-equilibrium homogeneous chemistry approach for the pyrolysis gas is presented, and results obtained using a legacy finite-rate chemistry model is reported. Although it is clear that such an approach is necessary, the lack of an appropriate chemistry model prevents that feature from giving meaningful results.

Then, a volume-averaged fiber-scale oxidation model is presented, based on the one previously developed by Lachaud et al. The present model, however, solves the momentum equation as well as the energy equation. Results based on a series of experimental test cases are presented.

Introduction

For extra-orbital missions, charring ablative materials have always been, and still remain, the primary choice for the design of atmospheric re-entry heat shields. These materials are usually made of a carbon matrix, usually composed of micro fibers, impregnated with a pyrolyzing resin, usually phenol.

With this type of material, the convective heating transmitted to the surface is dissipated by thermal and chemical decomposition. The gas emitted from the inner decomposition of the matrix is expelled into the free stream, thickening the boundary layer and pushing the bow shock away from the surface. This creates an additional protective gas layer at the surface but, more importantly, the chemical composition at the surface of the vehicle is changed considerably, which also attenuates the transmitted heat by modifying the thermal conductivity of the boundary layer, and allowing endothermic chemical reactions in that region.

As demonstrated in the past,[1–3] the composition of the pyrolysis gas in the boundary layer has an immediate impact on the heat flux attenuation on the surface of the vehicle. The usual assumption has been to consider that the pyrolysis gas is in chemical equilibrium when reaching the surface. Although that assumption might very well be true, it is however clear that the gas is not in chemical equilibrium when traveling through the charred ablator. The great majority of material response codes[4] use a chemical equilibrium assumption, both for simplicity and because of the lack of a validated model. This might lead to imprecisions in the evaluation of the efficiency of the ablator, and therefore increase the safety margin associated with the thickness of the heat shield at the design stage. Of course, this directly translates into a reduction of the usable payload, and an increase of operation cost.

*Assistant Professor, Senior Member AIAA. alexandre.martin@uky.edu

In the past, a few attempts have been made to come up with a comprehensive chemical nonequilibrium model: the first and most famous one dates from the early 70s, and was proposed by April.[5] The model was based on very specific reaction paths that were only applicable to the model. Most reactions are non-reversible, and lead to a decomposition of the phenolic gas that is not consistent with recent calculations.[6–8] Moreover, depending on the source used, the reactions are sometimes reversible,[9] sometimes not,[5,10] or are all homogeneous,[5,10] or involve solid carbon.[9] Recent attempt to use that model have not given satisfactory results, as pointed out in Ref. 11. Another study has come up with a new reaction set, but lack of available data has resulted in an un-correlated and uncalibrated model that does not have any basis in experimental study or careful study of the available reaction paths.[12]

Another very active area of research for ablative material is surface reaction. For charring ablators, it has been speculated that surface reaction does not occur on the surface of the material, but in a thin layer near the surface.[13] The ablator in this regions entirely pyrolyzes, leaving the carbon completely exposed to the surrounding gas. Because of the high porosity of the material, reacting gas from the outer flow, mostly oxygen, diffuse inside the layer, and reacts at the surface of the fibers, eroding them until they completely vanish.

In this context, it is evident that there is a blatant need to update and modernize past experiments, such as the one presented in Ref. 9, and propose new, validated pyrolysing chemistry and surface reactions model. In the recent year, the first steps of such a study has been underway,[14] and it is hopeful that this effort will lead to a more accurate description of the behavior of the chemically reacting pyrolysis gas, as well as fiber erosion. In the meantime, the current paper aims at preparing the numerical framework necessary to evaluate and complement the outcome of these experiments. In order to do this, a validated material response code is modified to 1) account for homogeneous chemical non-equilibrium for the pyrolysis gas, and 2) account heterogeneous reaction of the gas with the surface of the carbon fibers.

Material response code

Chemical equilibrium material response

The material response code used in the present study has been developed and validated over the last few years.[15] The code models chemical equilibrium gas flow through porous media by solving the following four conservation equations in one dimension:

Mixture Energy Equation

$$\frac{d}{dt}\int_{cv}\rho E dV - \int_{cs}\rho h v_{cs} dS + \int_{cs}\phi\rho_g h_g v_g dS \quad + \int_{cs}\dot{q}'' dA + \tilde{E}_{kin} = 0 \tag{1}$$

Solid Phase Equation

$$\frac{d}{dt}\int_{cv}\rho_s dV - \int_{cs}\rho_s v_{cs} dS - \int_{cv}\dot{m}_s''' dV = 0 \tag{2}$$

Gas Phase Continuity Equation

$$\frac{d}{dt}\int_{cv}\phi\rho_g dV - \int_{cs}\phi\rho_g v_{cs} dS + \int_{cs}\phi\rho_g v_g dS - \int_{cv}\dot{m}_g''' dV = 0 \tag{3}$$

Momentum Equation: Darcy's Law

$$\frac{\partial P}{\partial z} = -\frac{\mu}{K}\phi v_g \tag{4}$$

The first terms in Eqs. (1) to 3 account, respectively, for the energy, solid mass, and gas mass content, and the second term for the grid convection. The third terms in Eqs. 1 and 3 accounts for the gas flux, and the last terms in Eqs. 2 to 3, the source term. As for the fourth term of Eq. 1, it accounts for the heat conduction, and it is modeled according to Fourier's Law:

$$\dot{q}'' = -\kappa\frac{\partial T}{\partial z}$$

The kinetic energy $\tilde{E}_{kin}$ of the pyrolysis gas, which is mostly negligible, is obtained with:

$$\tilde{E}_{kin} = \frac{d}{dt}\int_{cv} \rho \frac{v_g^2}{2} dV + \int_{cs} \phi \rho_g \frac{v_g^2}{2} v_g dA - \int_{cs} \rho \frac{v_g^2}{2} v_{cs} dA$$

In theory, Darcy's law is only valid for porous flow. However, it is possible to adapt it for non porous media by adjusting the value of permeability. Since the average velocity of a steady, laminar and fully developed flow in a pipe of radius R is given by

$$\bar{v} = -\frac{\partial P}{\partial z}\frac{R^2}{8\mu}$$

and that $\phi = 1.0$ when the material is not porous, by analogy, it can be seen that Darcy's law can be valid by simply assuming that $K = R^2/8$.

In its current state, the code can account for multiple solid species, but only account for a single gas. The properties of this gas, such as viscosity and heat capacity, are therefore computed a priori, as a function of temperature only, using an equilibrium chemistry assumption. The atomistic mass fractions of the gas are determine by the resin decomposition as it is assumed that the decomposing solid will be transformed in this gas.

In order to adapt the code to account for nonequilibrium chemistry, modifications to the solid mass conservation equation and to the gas phase mass conservation equation need to be made. The first part is trivial, as the multi-material approach can easily be rewritten for multi-species. For instance, to model PICA, only two material species are needed: carbon and phenolic. The phenolic will be directly decomposing into the pyrolysis gas, as the carbon will have a source term (carbon deposition) and a destruction term (carbon oxidation).

The multi-species approach in the gas phase requires more subtle modifications, as well as more physical models. In these equations, all the solid material that is removed through pyrolysis is assumed to be transformed into the gas, at equilibrium. Mathematically, this simply means that $\dot{m}_g''' = -\dot{m}_s'''$. As there is only one gas, this 'transfer" is simple. However, if nonequilibrium chemistry is to be considered, the gas phase is composed of multiple species, each linked one to another through a set of chemical reactions.

Chemical non-equilibrium

In order to account for chemical reaction in the gas phase, the mass conservation equation now needs to account for inter-species diffusion as well as a gas phase chemical source term. The gas phase continuity equation, Eq. 3, therefore becomes:

$$\frac{d}{dt}\int_{cv} \phi \rho_{gk} dV - \int_{cs} \phi \rho_{gk} v_{cs} dS + \int_{cs} \phi \rho_{gk} v_g dS - \int_{cs} \phi J_k dS - \int_{cv} \left(\dot{m}_{gk}''' + \omega_k\right) dV = 0 \tag{5}$$

In this equation, k represents one of the species of the finite rate chemistry model; there is therefore such an equation for all the species considered, and $\sum_k \rho_{gk} = \rho_g$. The term $\dot{m}_{gk}'''$ relates to the mass fraction of the solid that is transfered to species k, and ω_k relates to the amount of species k that is created using the finite-rate chemistry model. The latter source term is evaluated by:

$$\omega_k = M_k \sum_{j=1}^{m} (\beta_{kj} - \alpha_{kj}) \left[k_{fj} \prod_{i=1}^{q} \left(\frac{\rho_i}{M_i}\right)^{\alpha_{ij}} - k_{rj} \prod_{i=1}^{q} \left(\frac{\rho_i}{M_i}\right)^{\beta_{ij}} \right]$$

where α_{ij} and β_{ij} are, respectively, the stoichiometric coefficients for product and reactants i of reaction j and M_j the molar mass of species j. The forward k_f and backward k_r rates are calculating using:

$$k_{f,b} = k_0 T^{-s} \exp\left(-E/RT\right) \tag{6}$$

in which the coefficient k_0, s and E are listed in Table 1, in a following section. The species mass diffusion, J_k, is modeled using Fick's Law:

$$J_k = -\rho \frac{D_k}{\eta}\frac{\partial Y_k}{\partial z}$$

where Y_l is the mass fraction of species k, and η the tortuosity. This equation is implemented in a way that enforces that the sum of all the diffusion fluxes are zero, if the models used to calculate the species diffusion D_k requires it.[16]

The energy equation also needs to be modified to account for the mass diffusion:

$$\frac{d}{dt}\int_{cv}\rho E dV - \int_{cs}\rho h v_{cs} dS + \int_{cs}\phi\rho_g h_g v_g dS \quad + \int_{cs}\dot{q}'' dA + \int_{cs}\phi\sum_k J_k h_{g_k} dA = 0 \tag{7}$$

Thermodynamical and Transport properties

The chemical properties of each individual species are evaluated using the thermodynamic curve fits obtained from Ref. 17. This provides a value for the heat capacity C_{Pk} of each species, as well as enthalpy h_k, heat of formation h_k^0 and entropy S_k. These values are also used to calculate the equilibrium values if reversible reactions are used in the finite-rate chemistry model. The single species viscosity μ_k and conductivity κ_k are obtained using curve fits compiled in Ref. 12. Because of the lack of data available for multi-component viscosity, the property of the gas mixture is evaluated using the simple approximation to the first term of the Chapman-Enskog expansion, Wilke's mixing rule:[18]

$$\mu = \sum_k \frac{X_k \mu_k}{\phi_k} \quad \text{and} \quad \kappa = \sum_k \frac{X_k \kappa_k}{\phi_k}$$

where X_k is the molar fraction and ϕ_k is given by:

$$\phi_k = \sum_r X_r \frac{\left[1 + \sqrt{\frac{\mu_k}{\mu_r}}\left(\frac{M_r}{M_k}\right)^{1/4}\right]^2}{\sqrt{8\left(1+\frac{M_k}{M_r}\right)}}$$

Because no binary collision data is used in this approach, the diffusion coefficient D_k is obtained using the constant Lewis Number approximation:

$$D_k = D = \frac{\text{Le } k}{\rho C_P}$$

Volume-averaged fiber-scale oxidation modeling

It has been shown that the so-called surface ablation, is more likely to be a volumetric phenomenon.[13] Lachaud has theorized, and later demonstrated that the oxygen from the surrounding flow actually penetrates the porous material over small distance, and oxidize the material from within. The recession rate, therefore, is not based on the macroscopic surface that is exposed to the flow field, but on the surface of the carbon fibers, and therefore on the porosity of the material. It is most probable that the rate of surface ablation is not driven by a series of competing surface rates. In this study, the chemical oxidation is therefore only modeled by using a single heterogeneous reaction:

$$\mathrm{C_{(s)}} + \mathrm{O_2} \longrightarrow \mathrm{CO_2}$$

Using the same volume-averaged approach laid down by Lachaud, the fiber recession phenomenon is integrated in the code. The reaction rate, as in Lachaud's work, is expressed as a constant k_f, and the diffusion flux of incoming oxygen is equivalent to the flux of outgoing carbon dioxide:

$$-J_{\mathrm{CO_2}} = J_{\mathrm{O_2}} = k_f C_{\mathrm{O_2}}$$

where $C_{\mathrm{O_2}}$ is the molar concentration of oxygen. Thus, the surface recession of an individual fiber of radius r is expressed in terms of the molar diffusion of carbon dioxide $J_{\mathrm{CO_2}}$ at the surface:

$$\dot{\mathbf{r}} = \Omega J_{\mathrm{CO_2}} \mathbf{n}$$

where $\Omega = M_c/\rho_c$ is the solid molar mass of the carbon, and $\mathbf{n}$ the normal vector to the surface of the fiber, pointing outward. Assuming that the fibers are perfectly cylindrical, and that they recess uniformly, this equation can be expressed in 1D as:

$$\frac{dr}{dt} = -\Omega k_f C_{O_2} \tag{8}$$

The volumetric approach used here assumes that the fibers enclosed in a control volume V_T all have the same initial radius, and are distributed homogeneously. The control volume can therefore be split into the volume occupied by the fibers V_f, and the volume "occupied" by the pores V_p. These can be expressed in terms of volume fraction:

$$\frac{V_f}{V_T} + \frac{V_p}{V_T} = \epsilon + \phi = 1$$

where ϵ is the fiber volume fraction, and ϕ the porosity. The volume occupied by N fibers of diameters of diameter r and length l_f are therefore given by $V_f = N\pi r^2 l_f$. As the fibers oxidize, the fiber volume fraction changes, and can be expressed as a function of the initial volume fraction:

$$\epsilon = \epsilon_0 \frac{r^2}{r_0^2}$$

In order to be included in the material response code, these relations have to be expressed in terms of the bulk density of the carbon matrix. This density can be expressed in terms of the mass of all fibers enclosed in the control volume:

$$\rho_s = \frac{m_f}{V_T} = \frac{N\pi r^2 l_f}{V_T}\rho_C = \epsilon\rho_C$$

where ρ_C is the density of solid carbon (not to be confused with the bulk density). The oxidation of fiber expressed in terms of bulk density change is therefore:

$$\frac{\partial \rho_s}{\partial t} = -\frac{\epsilon_0}{r_0^2} 2r\rho_C \frac{\partial r}{\partial t}$$

By using the parameter S_f, which represents the volumetric surface of occupancy by the fibers, and is defined as

$$S_f = \frac{N\pi 2Rl_f}{V_T} = 2\frac{\epsilon_0}{r_0^2} r, \tag{9}$$

as well as Eq. 8, this equation becomes:

$$\frac{\partial \rho_s}{\partial t} = -k_f S_f M_C C_{O_2} \tag{10}$$

or, if re-arranged in terms of ρ_s:

$$\frac{\partial \rho_s}{\partial t} = -2k_f \frac{M_C}{M_{O_2}} \frac{\rho_{O_2}}{r_0} \sqrt{\frac{\epsilon_0}{\rho_C}} \sqrt{\rho_s}$$

This expression can be solved analytically to give the evolution of the bulk density over time step Δt:

$$\rho_s^{(t)} = \left(\sqrt{\rho_s}^{(t-1)} - k_f \frac{M_C}{M_{O_2}} \frac{1}{r_0} \sqrt{\frac{\epsilon_0}{\rho_C}} \int_{(t-1)}^{(t)} \rho_{O_2} dt \right)^2 \tag{11}$$

The account of oxidation on the gas phase cannot be solved analytically, and must be integrated as a source term in Eq. 5:

$$\dot{m}'''_{O_2} = -\rho_{O_2} \frac{M_{O_2}}{M_{O_2}} S_f k_f \ , \quad \dot{m}'''_{CO_2} = \rho_{O_2} \frac{M_{CO_2}}{M_{O_2}} S_f k_f \tag{12}$$

It is to be noted that Eq. 10 can be re-written in the same form, to give:

$$\dot{m}'''_C = -\rho_{O_2} \frac{M_C}{M_{O_2}} S_f k_f$$

Numerical approach

The code solves Eqs. 5 and 7 implicitly on an arbitrary contracting grid employing Landau coordinates. Equation 2 is straightforward, and does not need to be solved numerically. As for Darcy's law, Eq. 4, it is explicitly solved for v_g and directly integrated in the gas-phase continuity equation.

Newton's method for nonlinear systems is used to solve each of the equations, and an iterative process is performed over the whole set until convergence is attained. This method, called block Gauss-Seidel, converges linearly, and is quite efficient when applied to a reduced set of equation. In the chemical equilibrium version of the code, only two equations needed to be solved numerically, and that method is appropriate. In the chemical non equilibrium version, the number of equations is dependent on the number of species, and therefore increases the iterative process immensely. Moreover, as finite-rate chemistry equations are very steep, the required time steps are also greatly reduced. Therefore, a problem that was solved in a few minutes in chemical equilibrium now takes hours to solve, even with a reduced number of species.

Instead of using block Gauss-Seidel on each of the $1 + N_S$ equation , where N_S is the total number of species, the method is only applied to the energy and the total gaseous mass conservation equation. However, in this second equation, the mass conservation of each species is solved at once, using the Newton method. Instead of solving for the total density, as was the case before, the mass conservation equation solves for each individual partial density. The Newton's method now requires the inversion of a block tri-diagonal system of equations, instead of a a simple tri-diagonal. This approach has numerous advantages, as it scales quite nicely ($\approx {N_S}^2$) with the number of species, it requires a limited number of changes in the code, and it retains the original structure.

For the fiber oxidation model, Eq. 11 is solved directly over time step Δt to calculate the solid decomposition and the surface function S_f. The latter quantity is then used as source terms in the gas phase equation (Eq. 5) by way of Eq. 12.

Boundary conditions

Because of the use of the block Gauss-Seidel approach, the only boundary condition that is necessary to modify is the one for the partial densities. Four different types of boundary conditions are applied. The first one, the impermeable wall, is the natural condition of the finite element approach, and therefore doesn't required anything to be set. The second type is used to set the properties of a surface exposed to a heat source: an external pressure is applied to the surface, and a zero gradient species concentration is imposed at the wall:

$$P_w = \rho_w R T_w = P_{\text{ext}}, \qquad \left(\frac{\partial Y_i}{\partial z}\right)_w = 0$$

In this equation, T_w is constant and is set (or provided for) by the boundary condition of the energy equation. This condition reduces to the so called "fixed pressure" boundary condition that was previously used in the code, when a single gaseous species in equilibrium was considered.

The third boundary condition imposes no gradient on the partial densities at the wall. Mathematically, this condition is:

$$\left(\frac{\partial \rho_i}{\partial z}\right)_w = 0$$

The fourth boundary condition imposes a mass fraction at the wall, as well as a pressure. This is enforced by way of the partial pressure of each individual species i:

$$\rho_{i_w} = \frac{M_i P_i}{R_u T}, \qquad P_i = P_{\text{ext}} \frac{Y_{i_{\text{ext}}}/M_i}{\sum_j Y_{j_{\text{ext}}}/M_j}$$

This type of boundary condition could be used for modeling experiments where a gas of known composition is forced through a test sample. This is, for instance, the type of condition required to reproduce April's experiment,[9] as well as the side-arm reactor experiments, both described in the following section.

Verifications

Multispecies model

In order to verify the approach, the code has been run with multiple species, using various species distribution, and comparing the results with the single species results. Since no reactions between the species are considered, and since mass is conserved, the results should be identical. For instance, in a 10 species test case, all gases have the same initial density, but each gas receives a fraction of the decomposed solid $\dot{m}_s'''$ proportional to their number (Gas 2 receives twice as much as Gas 1, Gas 3 three times as much, etc.). The geometry and condition of this test case are identical to one of the problems designed to test material response code.[19] As a boundary condition, the surface temperature linearly ramps for the first 0.1 s until it reaches 1644 K, at which point it stays constant. The material used in the simulation is TACOT.[19] The results, presented in Fig. 1 are shown after 5 seconds of simulated time.

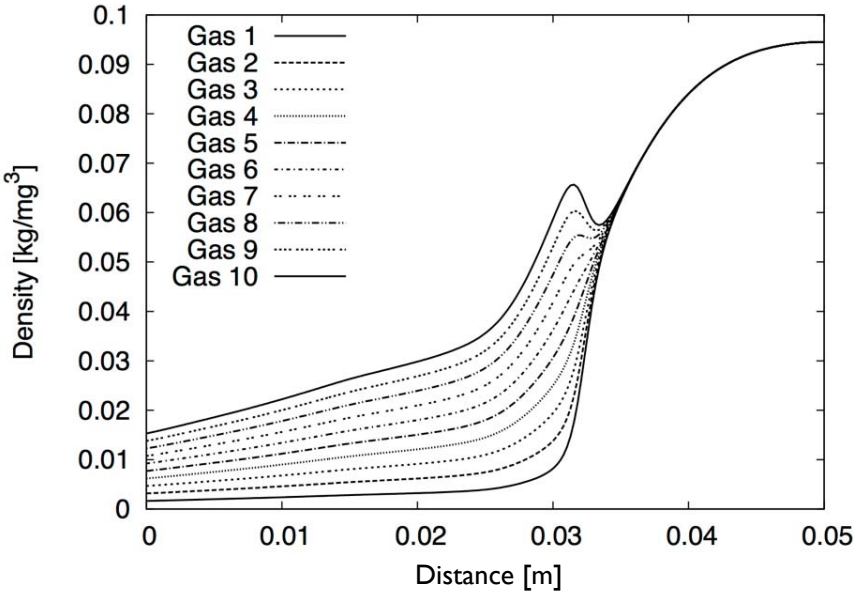

Figure 1. Multi-species verification: pyrolysis gas transformed into 10 non-reacting species

Another test-case is presented, which attempts to mimic the behavior of an initial gas being trapped in the ablator as it pyrolyzes. The initial gas is distributed with 60% in Gas 2, and 40% in Gas 3. The pyrolysis gas decomposes into Gas 3, Gas 4 and Gas 5, in the same proportional distribution as the previous test case. Gas 1 is left empty. The boundary condition is identical to the previous test-case. The results, after 5 seconds of exposure, are presented in Fig. 2. As can be seen, the pyrolysis gases essentially block the initial, non-reacting gas (Gas 2), and prevent it from being blown to the surface. This preliminary result is very interesting because it shows the importance of accounting for the initial gas when doing this type of simulation, since its presence can potentially change the chemical reactions in the ablator. It is to be noted that pyrolysis gas was transferred to Gas 3 to demonstrate the ability of the code to handle this behavior, and that Gas 1 was left untouched to show that a partial density of zero does not affect the stability of the code.

Chemistry model

It is possible to verify the chemistry implementation in the code by comparing it to an analytical solution for a simple problem.[20] By removing the dependence on temperature, and using a non-reacting third body

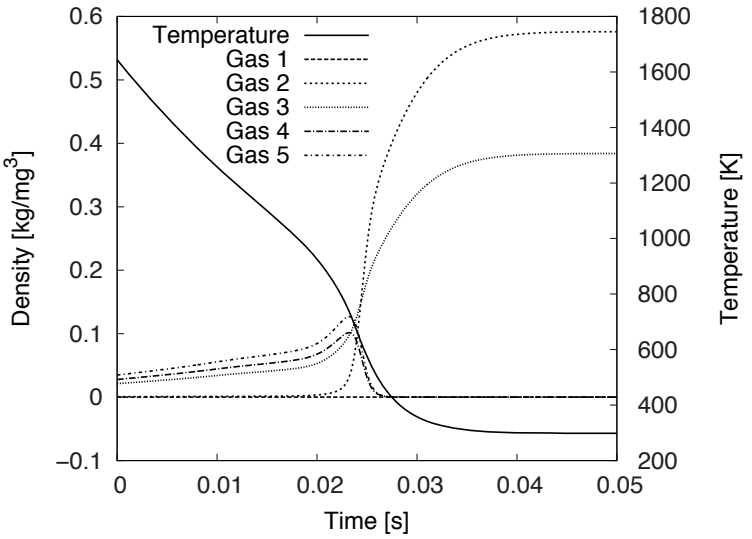

Figure 2. Temperature and partial densities of a multi-component non-reacting pyrolysis gas with an initial and different composition

species, an analytical solution can be obtained. The test-problem chosen is an O_2 gas at 10,000K. At that temperature, it is expected that the oxygen molecules will significantly dissociate into atomic oxygen. The third body non-reacting gas chosen is helium, which is irrelevant to the problem, although the gas is only allowed to dissociate when reacting with that gas. The initial density of O_2 and He are both 0.001 kg/m^3. The Arrhenius parameters for this reaction (Eq. 6) are $k_0 = 2.0 \times 10^{21}$, s = -1.5 and $E/R = 5.95 \times 10^4$. The results, compared to the analytical solution, are shown in Fig. 3.

A 5 species air model has also been tested, using the well known Park chemistry model (although used in thermal equilibrium). The initial gas is composed of an equal mixture of N_2-O_2, at an initial density of 0.02 kg/m^3, at 8000K. The results are shown in Fig. 4.

Results

Gas phase chemistry

Using the new reacting gas capabilities of the code, a test problem was modeled. This test-case is identical to the first test described in the validation section, but now uses fully reacting gases. The chemistry model, which only accounts for the homogeneous reactions of the pyrolysis gas, was devised by April.[5] This simple model, composed of 10 equations and 11 species, is presented in Table 1.

Because of previously reported problems with this model,[11] reaction 5 is omitted. Since no other reactions can produce CH_4, reaction 1 is also useless. The same reasoning causes the omission of reactions 2 and 3 as well. This reduces the number of species to 8: H_2, C_2H_2, C_6H_5OH (Phenol), C_6H_6, H_2O, CO, CO_2 and C. The test case modeled here is the same one that was described earlier, with the temperature at the wall at 1644 K.

The temperature and solid decomposition after 40 seconds of simulations is presented in Fig. 5, and the density of each of the species is presented in Fig. 6. Initially, the material is filled with H_2 at the external pressure. The pyrolysis gas, once decomposed from the solid state, is considered to be made from entirely of Phenol. Although this test-case is fictitious, and does not allow any comparison to experiments, it clearly indicates that the procedure described in the previous section works as expected, and does allow the efficient modeling of multi-species reacting pyrolysis gas in a porous charring ablator.

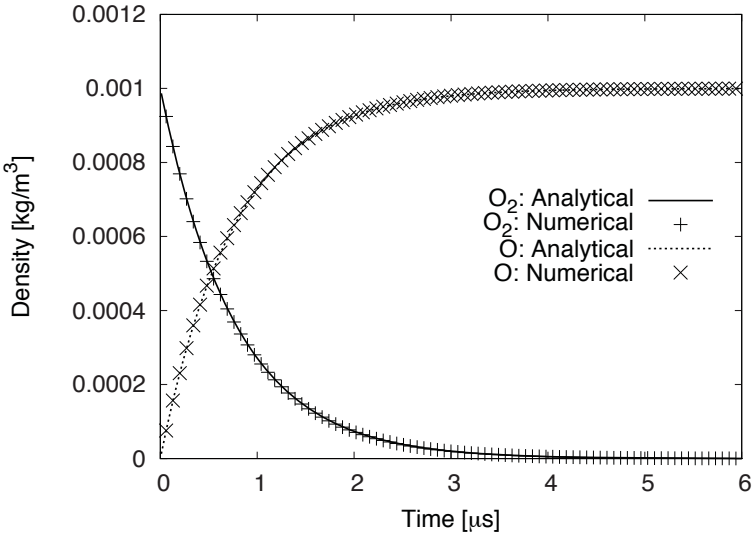

Figure 3. Time evolution of an O_2 gas at 10,000K

Fiber oxidation

This feature of the material response code has been integrated to model a very specific set of experiments performed at the NASA Ames sidearm reactor.[14] The test-case shown here somewhat reproduces the experimental conditions of one of these experiments. The sidearm reactor consist of a 2.2 cm diameter tube in which a FiberForm sample is introduced. The sample, 2.03 cm in length, completely fills the tube radially, which forces the gas through it. Before reaching the sample, the gas travels within a long pipe which ensure that it reaches a fully developed state, and that the temperature is not fluctuating. The specific case modeled here has the gas traveling at a mass flow rate of 2.149×10^{-6} kg/s, with a pressure at the inlet is at 12.8 kPa. The pressure at the back of the sample is set to 12.1 kPa, according to the experimental measurements. Since the code uses Darcy's law to model the velocity, this translates into a permeability of 1.367×10^{-10} m^2. The tortuosity is set to 1.15 for the initial state of the sample, and decreases linearly to 1.00 when the material reaches a porosity of 1.0. The initial porosity of the material has been measured at 0.9, and the bulk density to 184 kg/m^3. Fig 8 shows the mass flow rate through the sample, using those values, for a non-reacting sample.

In the free flow region, in front of the sample, the porosity is set to 1.0, and the permeability to 5.0×10^{-7} m^2. This is not exactly the value that would correspond to a radius of 0.011 m; however, setting such a high value for the permeability causes significant stability issues. A series of tests at various values, ranging from 1.0×10^{-6} up to 1.0×10^{-8} has shown that the results were not significantly affected by that approximation if the mass flow rate remains the same, which can be enforced by slightly decreasing the pressure at the outlet.

Another key aspect of the simulation is that a section of the tube must be modeled in order for a reasonable diffusion driven boundary layer to developed in front of the sample. This is necessary as the flow travels at such a small velocity (around 0.114 m/s) that the diffusion velocity is not negligible. This means that, as the sample oxidizes, a significant amount of CO_2 will diffuse in the opposite direction of the flow, therefore reducing the amount of available O_2. It is clear that the accuracy of the diffusion coefficients plays a significant role in the surface recession. For instance, using a reactivity of $k_f = 0.1$ m/s and a mass flow rate of 0.2 kg/s, the recession of the sample is presented in Fig. 7a). It can be seen that the diffusion of CO_2 is clearly affected by the boundary condition, and that the amount of O_2 available near the surface is quite high. The recession is therefore most probably overestimated in this case. For the same test case,

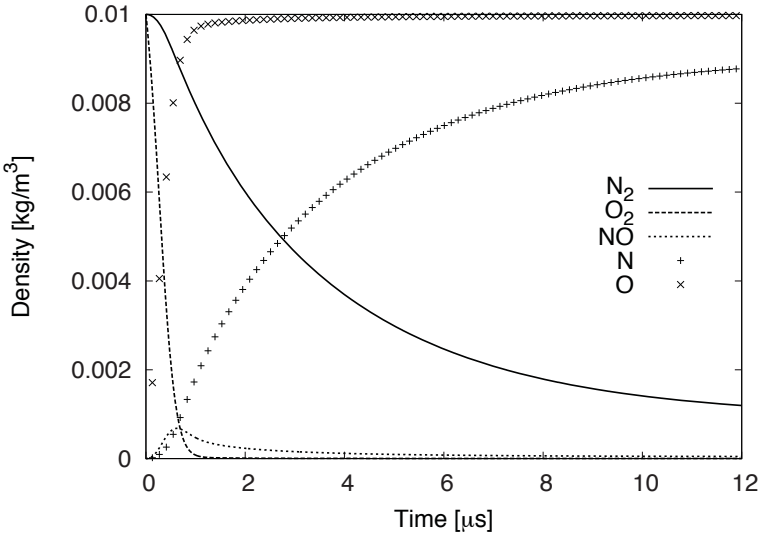

Figure 4. Time evolution of an N_2-O_2 gas mixture at 8000K

Fig. 7b shows the volume averaged radius in the sample. Finally, it is also clear that the simulation is erroneous in this case when looking at the velocity. Because the amount of oxygen is greatly overestimated, the rate of production of CO_2 is high enough that the flow is reversed. This situation means that the species concentrations are all guided by species diffusion, and no convection plays any role in the amount of oxygen in the sample. Fig. 9 illustrates that problem.

In order to ensure that the carbon dioxide sufficiently diffuses and that the boundary layer is not affected by the boundary condition, a lead length of 0.8 meter is modeled in front of the sample. Results of the full simulation are presented in Fig. 10, using a reactivity of $k_f = 0.01$ m/s, which is the one reported in Ref. 14. The results present a quantitative match with the experimental recession rate of 7 mm.

Since the code also solves the energy equation, results for the temperature of the gas are also presented. Because oxidation is an exothermic process, a rise in temperature it is expected to be observed. As shown on Fig. 11, this rise is significant, although it is most probably artificially high in the sample as the boundary condition at the exit forces the temperature to come down at the entrance level. This rise in temperature could explain why the reactivity reported in Ref. 14 is higher than expected: the sample is most probably several hundred degrees higher than the incoming gas.

Finally, it is also interesting to look at the oxygen penetration. Since the presented model solves the momentum equation, the gas velocity is calculated, and not inferred from the incoming mass flow rate. As can be seen on Fig. 10 oxygen is therefore pushed in much deeper then the 2 mm reported in Ref. 14.

From these preliminary results, it is clear that much more work is needed to model the sidearm reactor experimental campaign. It is also clear, however, that both the momentum equation and the energy equation must be solved to capture the physics of the problem. It is also possible that axisymmetric effects are importance, since the flow travels through the pipe at various axial velocities, and that the gas diffuses in all direction equally, when in the boundary layer. This might also potentially affect the recession rate.

Conclusion

Currently, most material response codes use equilibrium chemistry to model the effects of pyrolysis gas traveling inside a charring ablator. Finite-rate chemistry models proposed in the past are either outdated[5] or need further verification and validation.[12] This paper presents a new version of an existing material response

Table 1. Reaction and kinetics rate data of the April model

	Reaction formula	Rate Law [g-mol/cm^3]	k_0 [s^{-1}]	s	E [kcal/g-mol]
1	$CH_4 \rightarrow 0.5\ H_2 + 0.5\ C_2H_6$	$k_f[A]$	7.6×10^{14}	0	95.0
2	$C_2H_6 \rightarrow H_2 + C_2H_4$	$k_f[A]$	3.1×10^{14}	0	70.0
3	$C_2H_4 \rightarrow C_2H_2 + H_2$	$k_f[A]$	2.6×10^{8}	0	40.0
4	$C_2H_2 \rightarrow 2C{+}H_2$	$k_f[A]^2$	2.1×10^{10}	0	10.0
5	$C + 2H_2 \rightarrow CH_4$	k_f	2.0×10^{9}	0	17.0
6	$C_6H_5OH{+}H_2 \rightarrow H_2O{+}C_6H_6$	$k_f[A]$	2.0×10^{13}	0	45.0
7	$C_6H_6 \rightarrow 3\ C_2H_2$	$k_f[A]$	1.4×10^{9}	0	35.0
8	$C{+}H_2O \rightarrow CO{+}H_2$	$k_f[A][B]$	1.2×10^{12}	-1	82.0
9	$CO{+}H_2O \rightarrow H_2 {+}CO_2$	$k_f[A][B]$	1.0×10^{10}	0	30.0
10	$C + CO \leftrightarrow 2\ CO$	$k_f[A]$	1.0×10^{6}	-1	50.0
		$k_r[R]^2$	1.0×10^{-9}	0	61.0

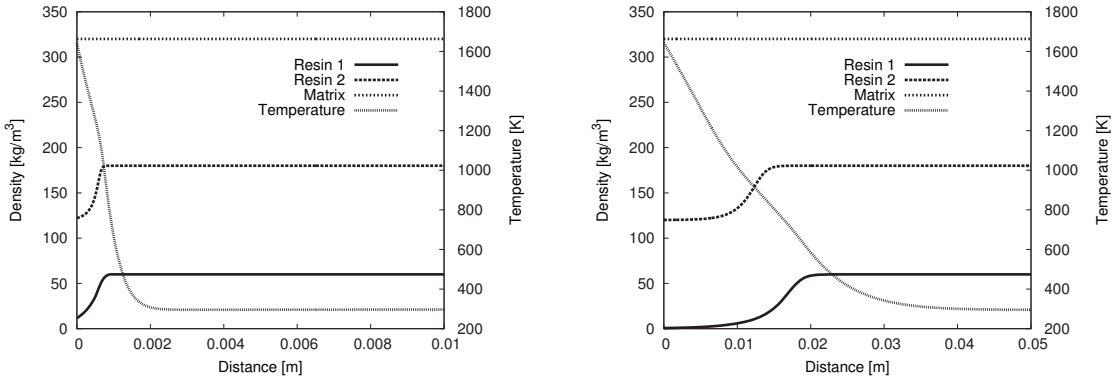

(a) 0.2 secondes of exposure

(b) 60 secondes of exposure

Figure 5. Temperature and solid densities in the TACOT ablator

code that will serve as a developing framework to build and validate a new comprehensive model, which will be based on ongoing experimental work.[14] The results shown using the outdated model clearly demonstrates the need for such a model.

The second feature demonstrate here, the volume-averaged fiber-scale oxidation model, also show significant improvement in terms of surface recession capabilities. Building on a previously developed model,[14] the new model also solves the energy and momentum equations. The results shows expected agreements with experiments and past results, and also demonstrates the importance of accounting for momentum and energy.

Acknowledgments

Financial support for this work was provided by NASA SBIR Phase-2 Award NNX10CC53P, and NASA Kentucky EPSCoR Award NNX10AV39A. The author would like to thank Dr. Sean Bailey at the University of Kentucky, as well as Dr. Jean Lachaud, at NASA Ames Research Center, for several useful discussions.

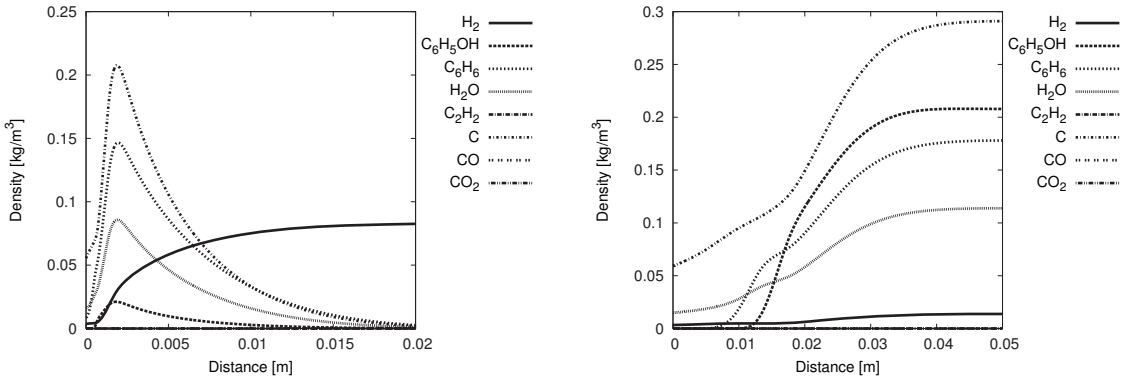

(a) 0.2 secondes of exposure

(b) 60 secondes of exposure

Figure 6. Partial densities of the pyrolysis gas in chemical nonequilibrium in the TACOT ablator

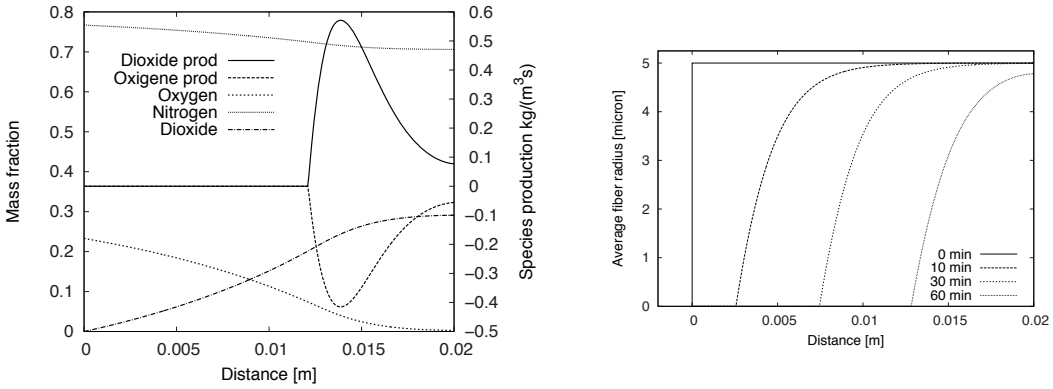

(a) Gas mass fraction and production rate after 60 minutes of exposure

(b) Fiber diameter

Figure 7. Time dependent properties inside the FiberForm sample for a mass flow rate of 0.2 mg/s and a fiber reactivity of $k_f = 0.1$ m/s

References

[1]Martin, A. and Boyd, I. D., "Assessment of carbon-phenolic-in-air chemistry models for atmospheric re-entry," *10th AIAA/ASME Joint Thermophysics and Heat Transfer Conference*, No. AIAA-2010-4656, Chicago, IL, June 28th to July 1st 2010.

[2]Martin, A. and Boyd, I. D., "CFD Implementation of a novel carbon-phenolic-in-air chemistry model for atmospheric re-entry," *49th AIAA Aerospace Sciences Meeting and Exhibit*, No. AIAA 2011-143, Orlando, FL, January 4-7 2011.

[3]Martin, A. and Boyd, I. D., "Modeling of heat transfer attenuation by ablative gases during Stardust re-entry," *50th AIAA Aerospace Sciences Meeting*, No. AIAA 2012-0814, Nashville, TN, January 9–12 2012.

[4]Lachaud, J., Magin, T. E., Cozmuta, I., and Mansour, N. N., "A short review of ablative-material response models and simulation tools," *7th European Symposium on Aerothermodynamics*, Brugge, Belgium, 2011.

[5]April, G. C., del Valle, E. G., and Pike, R. W., "Modeling reacting gas flow in the char layer of an ablator," *AIAA Journal*, Vol. 9, June 1971, pp. 1113–1119.

[6]Tran, H. K., Johnson, C. E., Rasky, D. J., Hui, F., Hsu, M., Chen, T., Chen, Y., Paragas, D., and L.Kobayashi, "Phenolic Impregnated Carbon Ablators (PICA) as Thermal Protection Systems for Discovery Missions," Tech. Rep. TM-110440, NASA, 1997.

[7]Brezinsky, K., Pecullan, M., and Glassman, I., "The Pyrolysis and Oxidation of Phenol," *J. Phys. Chem*, Vol. 102, No. 44, 1998.

[8]Horn, C., Roy, K., Frank, P., and Just, T., "Shock-Tube Study on the High-Temperature Pyrolysis of Phenol," *International Symposium on combustion*, Vol. 1, 1998, pp. 321–328.

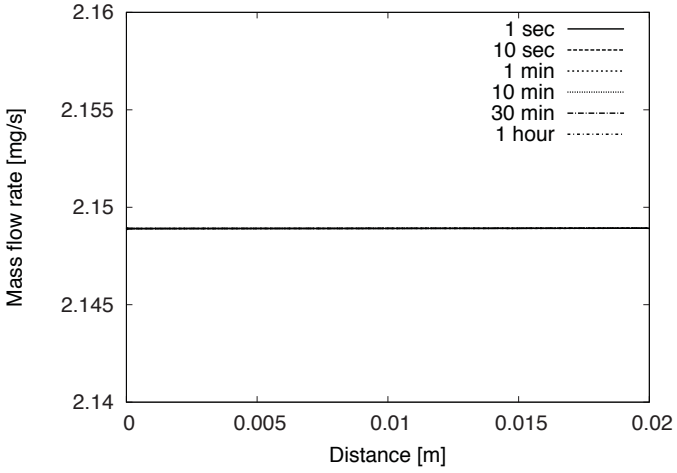

Figure 8. Mass flow rate inside a non-reacting FiberForm sample, at various times

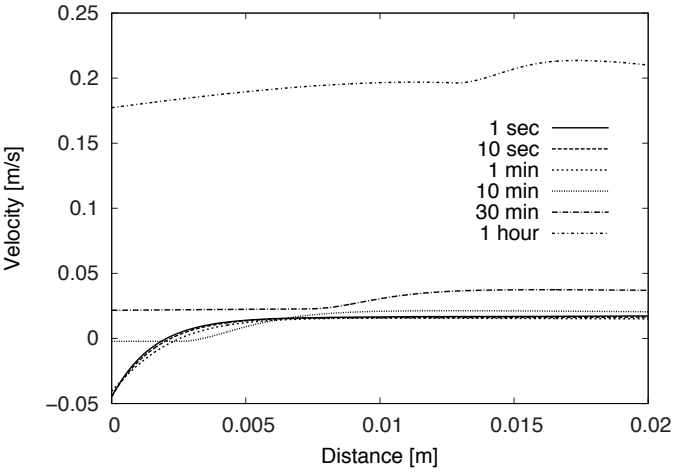

Figure 9. Velocity inside the FiberForm sample, as a function of time

[9]April, G. C., *Energy transfer in the char zone of a charring ablator*, Ph.D. thesis, Louisiana State University, Baton Rouge, LA, May 1st 1969.

[10]April, G. C., Pike, R. W., and del Valle, E. G., "On Chemical Reactions in the Char Zone during ablation," Contractor Report CR-1903, NASA Langley Research Center, 1971.

[11]Venkatachari, B. S., Cheng, G. C., Koomullil, R. P., and Ayasoufi, A., "Computational Tools for Re-entry Aerothermodynamics – Part II. Surface Ablation," *46th AIAA Aerospace Sciences Meeting and Exhibit*, AIAA-2008-1218, Reno, NV, Jan. 7-10 2008.

[12]Scoggins, J. B., *The Development of a Thermochemical Nonequilibrium Ablation and Pyrolysis Model for Carbon-Phenolic Thermal Protection Systems*, Master's thesis, North Carolina State University, 2011.

[13]Lachaud, J. and Mansour, N. N., "Microscopic scale simulation of the ablation of fibrous materials," *48th AIAA Aerospace Sciences Meeting and Exhibit*, No. AIAA 2010-984, Orlando, FL, 4-7 January 2010.

[14]Lachaud, J. R., Mansour, N. N., Ceballos, A., Pejaković, D., Zhang, L., and Marschall, J., "Validation of a volume-averaged fiber-scale model for the oxidation of a carbon-fiber preform," *42nd AIAA Thermophysics Conference*, No. AIAA 2011-3640, Honolulu, HI, 27-30 June 2011.

[15]Martin, A. and Boyd, I. D., "Non-Darcian behavior of pyrolysis gas in a thermal protection system," *Journal of Thermophysics and Heat Transfer*, Vol. 24, No. 1, Jan.-Mar. 2010.

[16]Sutton, K. and Gnoffo, P. A., "Multi-component diffusion with application to computational aerothermodynamics," *7th AIAA/ASME Joint Thermophysics and Heat Transfer Conference*, No. AIAA 1998-2575, Albuquerque, NM, June 15-18 1998.

[17]McBride, B. J., Gordon, S., and Reno, M. A., "Coefficients for calculating thermodynamic and transport properties of individual species," Technical Memorandum TM-451, NASA, 1993.

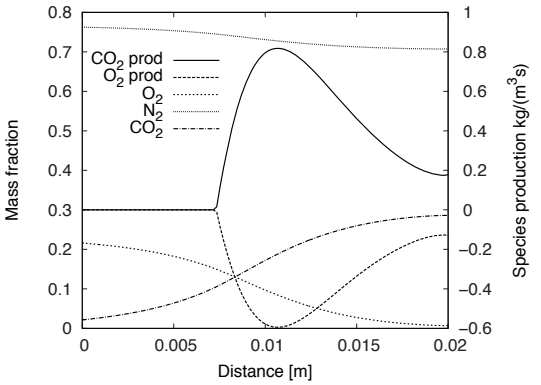

(a) Gas mass fraction and production rate after 60 minutes of exposure

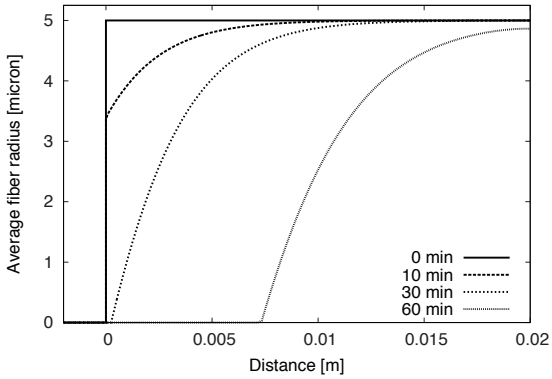

(b) Fiber diameter

Figure 10. Time dependent properties inside the FiberForm sample for a mass flow rate of 2.149 mg/s and a fiber reactivity of $k_f = 0.01$ m/s

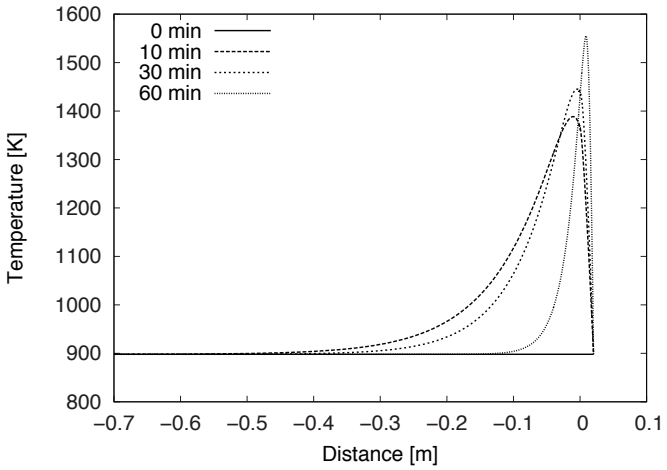

Figure 11. Temperature inside the FiberForm sample, as a function of time

[18]Wilke, C., "A viscosity equation for gas mixtures," *J. Chem. Phys.*, Vol. 18, No. 4, 1950, pp. 517–519.

[19]Lachaud, J., Martin, A., Cozmuta, I., and Laub, B., "Ablation test-case series 1," *4th AFOSR/SNL/NASA Ablation Workshop*, 2010.

[20]Zhang, H.-B., McDonough, J. D., and Martin, A., "Implementation, verification, and validation of chemical nonequilibium in a hypersonic CFD code," *37th Dayton-Cincinnati Aerospace Sciences Symposium*, Dayton, OH, March 6 2012.